A Rhombic Dodecahedral Honeycomb Structure with Cation Vacancy Ordering in a γ-Ga_2O_3 Crystal

Masanori Mitome[*, †], *Shigemi Kohiki*[‡], *Takuro Nagai*[§], *Keiji Kurashima*[§], *Koji Kimoto*[§], *Yoshio Bando*[†]

[†] International Center for Materials Nanoarchitectonics, National Institute for Materials Science, 1-1 Namiki Tsukuba Ibaraki 305-0044, Japan

[‡] Department of Materials Science, Kyusyu Institute of Technology, 1-1 Sensui Tobata Kitakyusyu 804-8550, Japan

[§] Advanced Key Technologies Division, National Institute for Materials Science, 1-1 Namiki Tsukuba Ibaraki 305-0044, Japan

MITOME.Masanori@nims.go.jp

RECEIVED DATE

TITLE RUNNING HEAD: Rhombic dodecahedral honeycomb in γ-Ga_2O_3 crystal

ABSTRACT

The crystal structure of a γ-Ga_2O_3 layer grown epitaxially on an MgO substrate by a vapor phase transport method was investigated by transmission electron micrscopy, electron diffraction, and scanning transmission electron microscopy with aberration correctors. Some forbidden reflections were excited in electron diffraction patterns by double reflection from the vicinity of the substrate interface. Phase boundaries are observed in atomic column images using high angle annular dark field images. A structure model is proposed to explaine the experimental results. Cation vacancy ordering is introduced in the structure model to distort the γ-Ga_2O_3 crystal lattice along one axis and reduce the lattice mismatch with the substrate. Some grains are formed and alter the directions to reduce the distortion for the other axis. The grains are stacked with {110} phase boundaries, and form a rhombic dodecahedral honeycomb. The rhombic dodecahedral honeycomb structure model with cation vacancy ordering is stabilized by the lattice mismatch between the γ-Ga_2O_3 crystal and the MgO substrate, and it disappears at a depth of 170 nm from the interface.

KEYWORDS: γ-Ga_2O_3, defect spinel structure, Epitaxial growth, Cation vacancy ordering, Rhombic dodecahedral honeycomb

Introduction

Gallium oxide (Ga_2O_3) is one of the most attractive wide band gap materials because of its transparerency, thermal and chemical stability and it is expected to find wide application to optoelectronics devices.[1] Five polymorphs are known for Ga_2O_3, that is, the α, β, γ, δ and ε forms.[2] The only stable form is the β form which has a monoclinic structure; the other forms transform into the β form at high temperature.[3] The stable β form has been extensively investigated, but the properties of the other forms are still poorly understood.

It has been reported that the metastable γ form shows some unexpected properties, that is blue litght emission from nanocrystals,[4] room temperature ferromagnetism on Mn doping,[5] and selective catalytic reduction of NO in γ-Ga_2O_3-Al_2O_3 system.[6] The metastable γ form therefore might be a more attractive material than the stable β form.

Basically the γ form has a cubic defect spinel-type structure with the lattice constant a = 0.822 nm and the space group $Fd\bar{3}m$.[7] Since the γ form was often synthesized as nanoparticles by a sol-gel method, the crystal size was too small to investigate the structure in detail, *i.e.* surface structure, crystal defects and so on. Recently, epitaxial growth of the γ form has been successful on MgO[8] or sapphire substrates.[9] We have observed some forbidden reflections from the γ form grown on an MgO substrate by transmission electron diffraction (TED) analysis,[10] but their origin was unclear. In this paper, we report details of the structure investigated by high resolution transmission electron micoroscopy (TEM), scanning transmission electron microscopy (STEM) and an *ab inito* energy calculation.

Experimental Methods

The Ga_2O_3 film was synthesized by a vapor phase transport method in a horizontal furnace.[8] A β-Ga_2O_3 powder in an alumina source boat and an MgO (001) substrate coated with a thin Au layer were loaded in the furnace. The gold particles play the role of catalysts in a vapor-liquid-solid (VLS) mechanis.[11] The source boat was heated up to 1200 °C at a rate of 10 °C/min and the substrate

temperature rose to 640 °C. A gas mixture (95% N_2 and 5% H_2) was flowed from the source to the substrate during the heating process. The film thickness was controlled by the processing time.

When the source boat was cooled after arriving at the mximum temperature, thin β-Ga_2O_3 nanocolumns had grown on the substrate. The growth direction was identified as the [001] orientation by TEM and TED analysis.[10] The γ-Ga_2O_3 layer could be obtained by keeping the system at the maximum temperature for 3 hours. The γ-Ga_2O_3 layer was formed at the interface with the substrate, while thick β-Ga_2O_3 nanorods grew on the surface.

A thin specimen for TEM observation was prepared by a focused ion beam (FIB) technique with a Hitachi FB-2000A. A small 10 μm wide piece was picked up from the specimen and was attached on a metal lift-out grid. Initially the piece was thinned to 70 nm by FIB with 30 keV Ga ions. It was thinned additionally by low energy Ar ion milling with a Fischione Model 1040 (NanoMill). A surface damage layer introduced by the FIB process was completely removed by Ar ion milling at a low energy of 500 eV.[12]

TEM and TED observation was performed using a JEOL JEM-3100FEF with a 300 keV acceleration voltage,[13] and STEM observation was performed with a FEI Titan^3 with aberration correctors and a monochoromater.[14]

Results

Fig. 1(a) shows a TEM image of a specimen thinned by FIB and low energy Ar ion milling and Fig. 1(b)-(d) are selected area electron diffraction patterns taken from the areas shown by circles in Fig. 1(a). The diffraction spots in Fig. 1(b) and 1(d) can be assigned to γ-Ga_2O_3 with a space group $Fd\bar{3}m$ and the MgO substrate, respectively. On the other hand, some forbidden reflections, for example (001), (002), (003), (012), (023) and so on, were excited in Fig. 1(c), but (011), (031) and (033) are not seen. Furthermore, streak lines were observed along the <110> reflection in Fig. 1(c). These suggested the presence of stacking faults or twins on the {110} planes.

Such a faulted structural phase is clearly differentiated from the usual $Fd\bar{3}m$ structure at the interface shown by an arrow in Fig. 1(a). It is not that the faluted structure fades out gradually on moving away from the substrate interface. The thickness of the faulted structure was 170 nm. This type of faulted structure has not been reported for the γ form grown on a sapphire substrate.[9]

Fig. 2(a) shows a high magnification TEM image of the faulted structure. This area was thinned by Ar ion and high energy electron beam and its width was 16 nm. The thickness in this area was probably equivalent to, or a little thicker than, the width, and thus it can be estimated as about 20 nm. To clarify the features, the image contrast was emphasized and shown with pseudo colors in Fig. 2(b). Some distinctive contrast can be seen in Fig. 2(b); high contrast column image areas indicated by H in Fig. 2(c) and low contrast areas L that surround the H areas. The square lattice in the H areas can be assigned to {022} reflections from the γ form. On the other hand, long periodic fringes appear in the L areas as shown by arrows in Fig. 2(b), and the periodicity corresponds to {001} reflections that are forbidden reflections for the usual γ form. The distinctive contrast suggests that small grains of 4-5 nm are connected with twin boundaries. Since the {110} twin boundary in a $Fd\bar{3}m$ structure corresponds to a phase boundary, long periodic fringes may appear when two grains connected by the twin boundary are overlapped.

Fig. 3 shows high angle annular dark fileld (HAADF) images taken by STEM with two kinds of incidence, [010] and [110]. The HAADF images can be interpreted as incoherent images, and thus every atomic column appears with bright contrast. The insets show gallium sites in a γ-Ga_2O_3 crystal structure. The yellow and green spheres indicate tetragonal and octahedral positions, respectively. The atomic arrangements in a unit cell are shifted from the lower regions to the upper regions. The images in the intermediate region can be interpreted as overlaps of both atomic arrangements in the lower and upper regions. This also supports the thesis that phase boundaries formed at the grain boundaries in the faulted structure.

Discussion

The structure of the γ form is usually described as a defect spinel structure like γ-Al_2O_3 with a lattice constant a = 0.822 nm. A spinel cubic cell has 32 oxygen atom sites and 24 cation sites in tetrahedral and octahedral positions, but $2\frac{2}{3}$ cation vacancies must be introduced to satisfy the Ga_2O_3 stoichiometry. If the vacancies occupy the specific positions regularly, the crystal symmetry is reduced from $Fd\bar{3}m$ and forbidden reflections like as (002) and (024) might be excited.

From *ab initio* calculations, it has been reported for both γ-Al_2O_3[15] and γ-Ga_2O_3[16] that the total energy is minimized when all the vacancies are located at specific octahedral positions that are furthest from each other. However, the energy difference between the possible vacancy configurations is too small after the structure optimization to conclude that the minimum energy structure is formed in the actual crystals at a finite temperature. Generally it is thought that the vacancies occupy both the tetrahedral and octahedral positions randomly to form the $Fd\bar{3}m$ symmetry.

There is some room created for the vacancies to occupy the specific positions when the crystal is distorted by the lattice mismatch between the crystal and the substrate. Since the substrate MgO has a cubic rock salt structure with the lattice constant of 0.421 nm that is 2.4% longer than one half of the lattice constant of γ-Ga_2O_3, some distortion should be introduced in the vicinity of the interface.

An optimized structure has been evaluated by an *ab initio* calculation for the minimum energy vacancy configuration that was predicted from the previous theoretical studies.[15, 16] Following the previous studies, we also used a supercell that is three times the size of the primitive cell of the cubic spinel structure. The supercell contains 24 oxygen atoms, 16 gallium atoms, and two cation vacancies, and the cation vacancies occupy the octahedral positions that are furthest away from each vacancy. The distance between the vacancies is 0.769 nm before the structure optimization. The calculation was performed with the ABINIT code[17] and a pseudo potential based on the generalized gradient approximation.[18]

The optimized supercell after the minimum energy calculation was converted into a cubic like unit cell, and the optimized lattice constants were obtained as $a = b$ = 0.8211 nm, c = 0.840 nm, $\alpha = \beta$ = 89.75°, and γ = 91.42°. The value of a and b are almost unchanged from the original cubic lattice

constant of 0.822 nm, but *c* is expanded by +2.1%, a value that is quite close to twice the lattice constant for MgO. The lattice mismatch between the γ-Ga_2O_3 and the MgO substrate can be relaxed for one axis by setting the elongated *c* axis parallel to the MgO [100] or [010] axis, though the lattice is still mismatched along the other axis normal to the *c* axis.

To reduce the distortion caused from the lattice mismatch, some grains could be formed. The elongated *c* axes of the γ-Ga_2O_3 grains are directed along the MgO [100] and [010] axes alternately, and these grains are connected with {110} interfaces. The structure model is schematically drawn in Fig. 4. The black square mesh in Fig. 4(a) represents an MgO (001) surface where oxygen atoms arrange in a square lattice. Oxygen atoms in a γ-Ga_2O_3 crystal also form a face-centered cubic arrangement, and the (001) surface can be represented by the red or blue lattices in Fig. 4(a). Here, the red square mesh is expanded toward the [010] direction of the MgO substrate and the lattice distance is matched to the MgO lattice; the blue square mesh is expanded toward the [100] direction similarly. These square meshs are arranged on the MgO substrate with alternate tiling, as shown in Fig. 4(b). The MgO and γ-Ga_2O_3 lattices match each other in the four areas shown by red circles in Fig. 4(b) and on vertical and horizontal bands connecting the red circles, while they mismatch around areas shown by green circles.

While the grains in this structure model are connected with {110} interfaces, {110} twin boundaries is also suggected by the TED pattern, the high resolution TEM image and the HAADF image. There are 12 equivalent {110} planes in a cubic structure, and a crystal grain truncated by these equivalent {110} planes forms a rhombic dodecahedron, as shown in Fig. 5(a). The rhombic dodecahedron is one of the polygons that can fill a 3D space without any gaps. The space tessellation is known as a rhombic dodecahedral honeycomb, where rhombic dodecahedrons are stacked on each other with face-centered cubic packing (see Fig. 5(b)).

According to the rhombic dodecahedral honeycomb structure model with cation vacancy ordering, the TEM images and TED patterns were simulated by the multi-slice method[19]. The supercell size used in the simulation was 11.6 nm x 11.6 nm and the thickness was 16.4 nm that was devided into thin slices 0.82 nm in thickness. In the simulated image shown in Fig. 6(a), some square high contrast

regions are surrounded by lower contrast boundary regions, and long periodic fringes are seen in the lower contrast boundary regions. These features correspond to those observed in the TEM image in Fig. 2. In the simulated diffraction pattern shown in Fig. 6(b), some forbidden (001), (002), (003), and (012) reflections and the streak lines along the <110> reflection were reproduced. This rhombic dodecahedral honeycomb model with cation vacancy ordering explains all the experimental results.

Conclusions

A structural model was proposed to explain the forbidden reflections observed from the vicinity of the interface between a γ-Ga_2O_3 layer and an MgO substrate. Cation vacancy ordering is introduced to reduce the lattice mismatch for one axis and some grains are formed in alternating 90° directions to reduce the distortion in the other axis. The grains are surrounded by {110} twin boundaries and form a rhombic dodecahedron. Finally, the rhombic dodecahedral grains are stacked to form a honeycomb. This structure model consistently explains all the experimental results. The sturucture is formed to reduce the 2.4% lattice mismatch between the γ-Ga_2O_3 crystal and the MgO substrate, and thus it is only stable on the substrate.

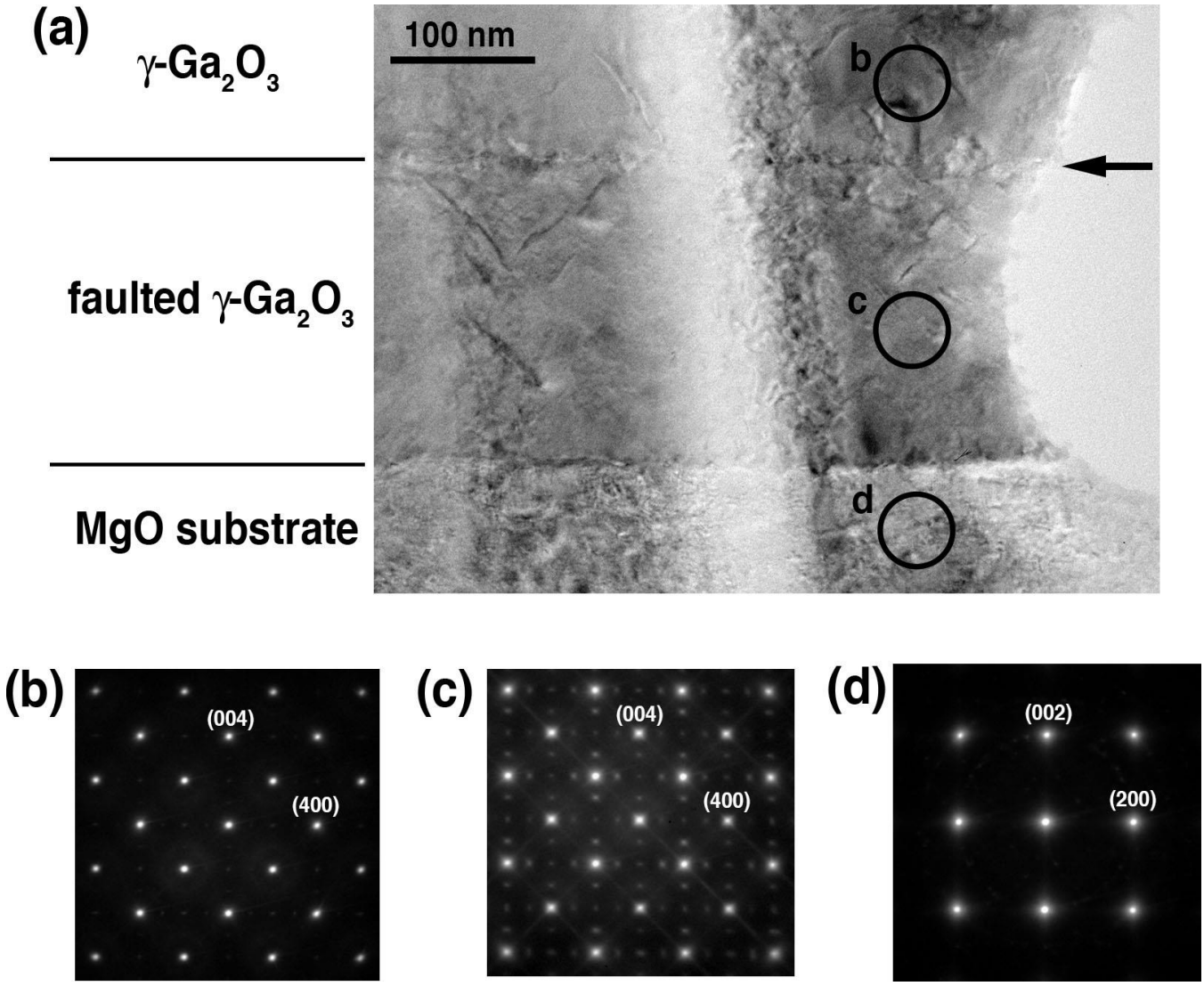

Figure 1. A transmission electron microscope image (a) of a γ-Ga_2O_3 layer grown epitaxially on an MgO substrate. Selected area electron diffraction patterns (b)-(d) taken from areas circled in (a).

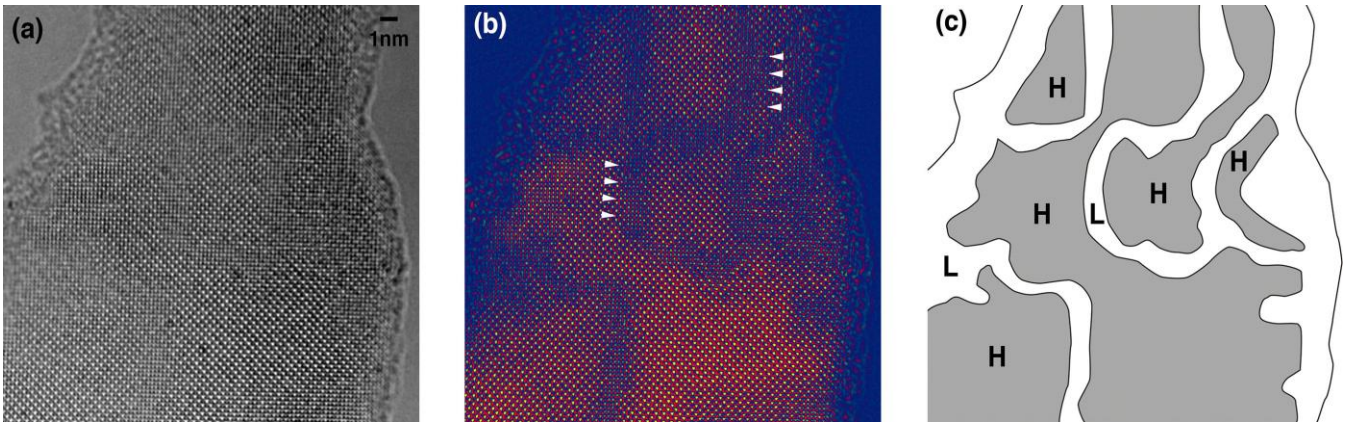

Figure 2. A high resolution transmission electron microscope image of a faulted γ-Ga_2O_3 layer (a). The contrast was emphasized and shown with pseudo colour in (b), and some distinctive contrast areas are shown schematically in (c).

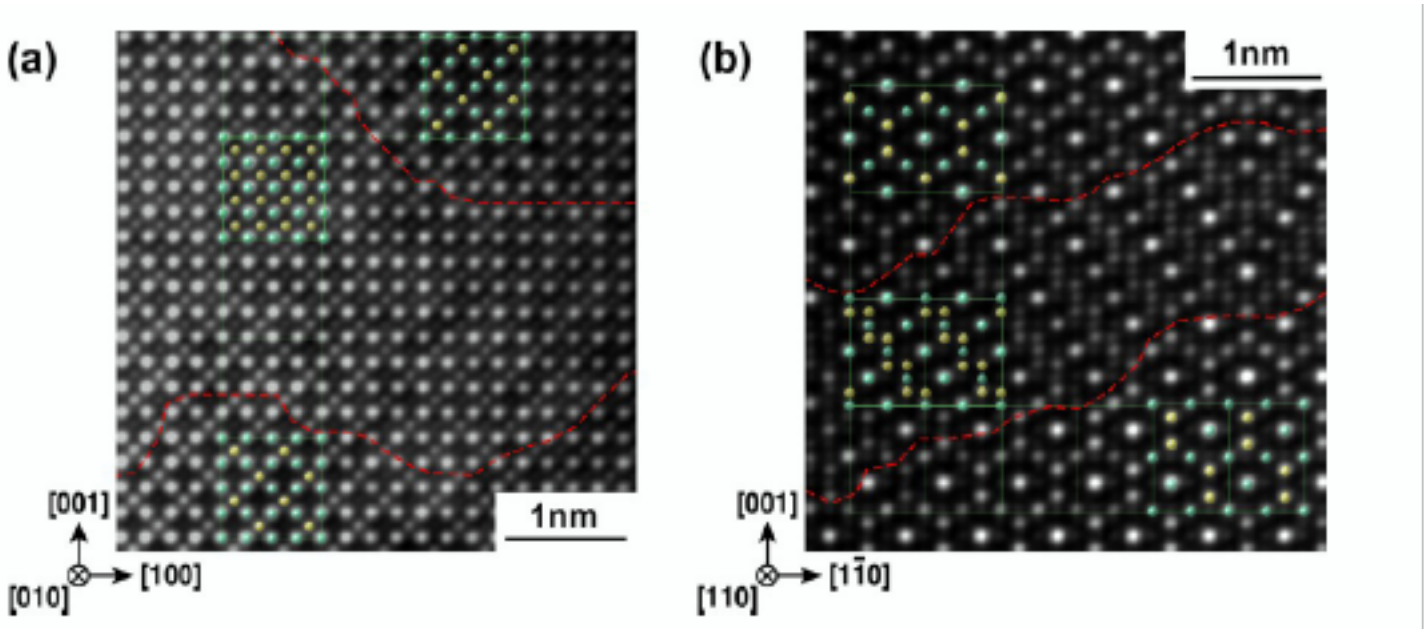

Figure 3. High angle annular dark field images of a faulted γ-Ga_2O_3 layer seeing from a [010] (a) and a [110] axis. The insets show gallium sites in a γ-Ga_2O_3 crystal structure. The green and yellow spheres indicate octahedral and tetragonal sites, respectively. The crystal lattices between an upper and lower sides are shifted, and there is a phase boundary.

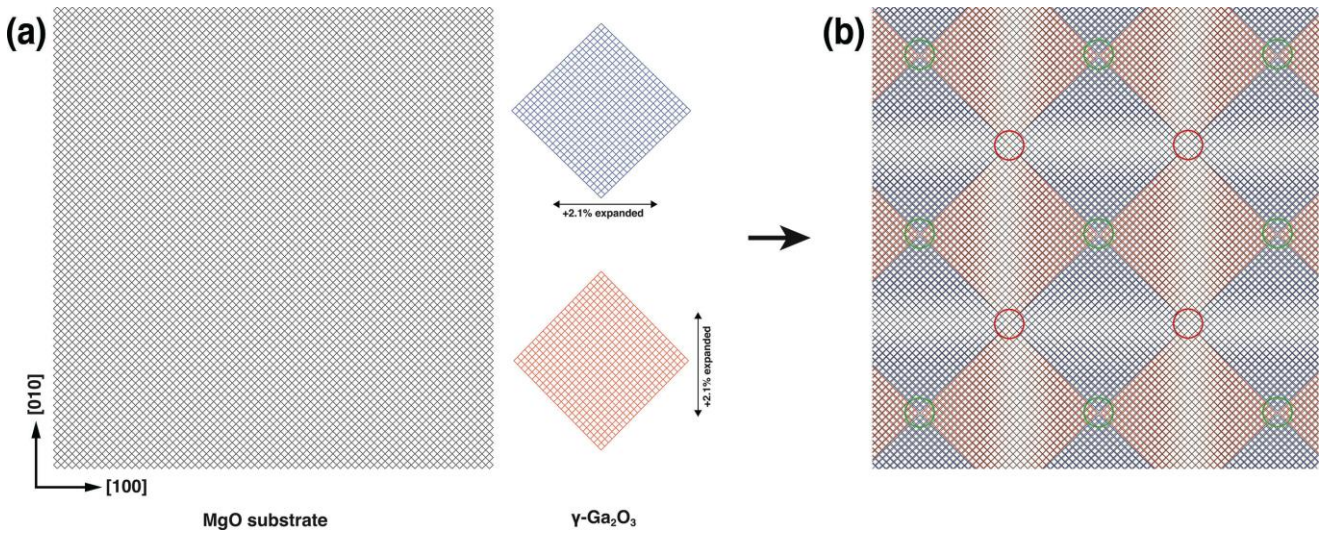

Figure 4. The grain stacking structure model. The black mesh represents the MgO substrate, and blue and red meshes represent a γ-Ga_2O_3 layer, which are expanded respectively along one axis in (a). The red and blue meshes are tiled alternately on the black mesh in (b).

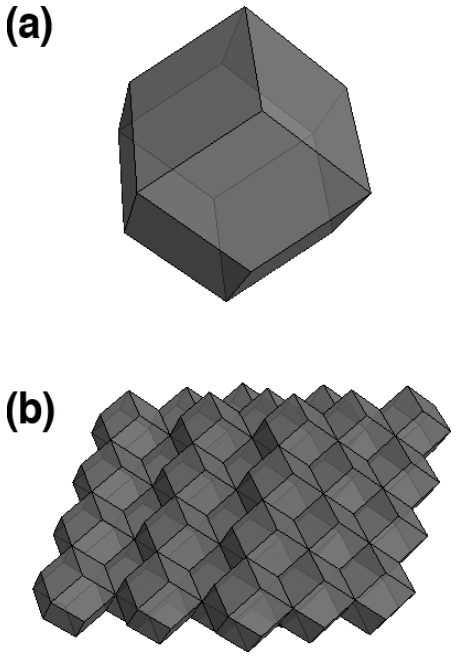

Figure 5. A rhombic dodecahedron (a), and a rohombic dodecahedral honeycomb (b).

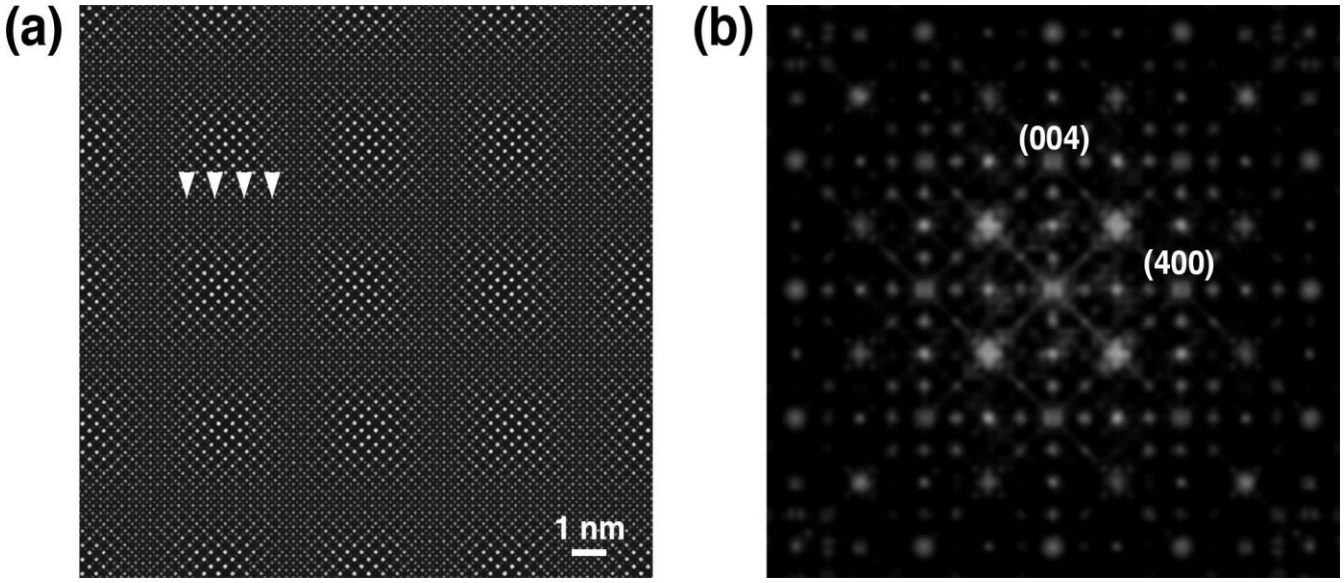

Figure 6. A simulated electron microscope image (a) and a simulated electron diffraction patterns (b) for a rhombic dodecahedral honeycomb with cation vacancy ordering.

REFERENCES

(1) (a) Ueda, N.; Hosono, H.; Waseda, R.; Kawazoe, H. *Appl. Phys. Lett.* **1997**, 70, 3561. (b) Orita, M.; Ohta, H.; Hirano, M.; Hosono, H. *Appl. Phys. Lett.* **2000**, 77, 4166.

(2) Roy, R.; Hill, V. G.; Osborn, E. F. *J. Am. Chem. Soc.* **1952**, 74, 719.

(3) Zinkevich, M; Adkinder, F. *J. Am. Ceram. Soc.* **2004**, 87, 683.

(4) (a) Chen, T.; Tang, K. *Appl. Phys. Lett.* **2007**, 90, 053104. (b) Huang, C-C.; Yeh, C-S. *New J. Chem.* **2010**, 34, 103. (c) Wang, T.; Farvid, S. S.; Abulikemu, M.; Radovanovic, P. V. *J. Am. Chem. Soc.* **2010**, 132, 9250.

(5) Hayashi, H.; Huang, R.; Ikeno, H.; Oba, F.; Yoshioka, S.; Tanaka, I. *Appl. Phys. Lett.* **2006**, 89, 181903.

(6) Takahashi, M.; Inoue, N.; Nakatani, T.; Takeguchi, T.; Iwamoto, S.; Watanabe, T.; Inoue, M. *Appl. Catal. B-Environ.* **2006**, 65, 142.

(7) (a) Pohl, K. *Naturwiss.* **1968**, 55, 82. (b) Areán, C. O.; Bellan, A. L.; Mentruit, M. P.; Delgado, M. R.; Palomino, G. T. *Microporous Mesoporous Mat.* **2000**, 40, 35. (c) Zinkevich, M.; Morales, F. M.; Nitsche, H.; Ahrens, M.; Rühle, M.; Zldinger, F. *Z. Metallkd.* **2004**, 95, 756.

(8) Hori, K.; Fukuta, M.; Shimooka, H.; Kohiki, S.; Shishido, T.; Oku, M.; Mitome, M.; Bando, Y. *J. Alloy. Compd.* **2005**, 390, 261.

(9) Hayashi, H.; Huang, R.; Oba, F.; Hirayama, T.; Tanaka, I. *J. Mater. Res.* **2011**, 26, 578.

(10) Mitome, M.; Kohiki, S.; Hori, K.; Fukuta, M.; Bando, Y. *J. Cryst. Growth* **2006**, 286, 240.

(11) Wagner, R.S.; Ellis, W.C. *Appl. Phys. Lett.* **1964**, 4, 89.

(12) Mitome, M. *Microscopy,* **2013**, 62, 321.

(13) Mitome, M.; Bando, Y.; Golberg, D.; Kurashima, K.; Okura, Y.; Kaneyama, T.; Naruse, M.; Honda, Y. *Microsc. Res. Tech.* **2004**, 63, 140.

(14) Kimoto, K.; Kurashima, K.; Nagai, T.; Ohwada, M.; Ishizuka, K. *Ultramicroscopy* **2012**, 121, 31.

(15) Gutiérrez, G.; Taga, A.; Johansson, B. *Phys. Rev. B* **2001**, 65, 012101.

(16) Yoshioka, S.; Hayashi, H.; Kuwabara, A.; Oba, F.; Matsunaga, K.; Tanaka, I. *J. Phys.: Condens. Matter.* **2007**, 19, 346211.

(17) (a) Gonze, X.; Amadon, B.; Anglade, P.-M.; Beuken, J.-M.; Bottin, F.; Boulanger, P.; Bruneval, F.; Caliste, D.; Caracas, R.; Côté, M.; Deutsch, T. Genovese, L.; Ghosez, Ph.; Giantomassi, M.; Goedecker, S.; Hamann. D.R.; Hermet, P.; Jollet, F.; Jomard, G.; Leroux, S.; Mancini, M.; Mazevet, S.; Oliveira, M.J.T.; Onida, G.; Pouillon, Y.; Tangel, T.; Rignanese, G.-M.; Sangalli, D.; Shaltaf, R.; Torrent, M.; Verstraete, M.J.; Zerah, G.; Zwanziger, J.W. *Computer Phys. Commun.* **2009**, 180, 2582. (b) Gonze, X.; Rignanese, G.-M.; Verstraete, M.; Beuken, J.-M.; Pouillon, Y.; Caracas, R.; Jollet, F.; Torrent, M.; Zerah, G.; Mikami, M.; Ghosez, P.; Veithen, M.; Raty, J.-Y.; Olevano, V.; Bruneval, F.; Reining, L.; Godby, R.; Onida, G.; Hammann, D.R.; Allan, D.C. *Z. Kristallogr.* **2005**, 220, 558.

(18) Perdew, J.P.; Burke, K.; Ernzerhof, M. *Phys. Rev. Lett.* **1996**, 77, 3865.

(19) Cowley, J. M.; Moodie A. F. *Acta Cryst.* **1957**, 10, 609.